Using lake sediment archives to improve understanding of flood magnitude and frequency: Recent extreme flooding in northwest UK

R.C. Chiverrell,[1]* (iD) D.A. Sear,[2] (iD) J. Warburton,[3] (iD) N. Macdonald,[1] D.N. Schillereff,[4] J.A. Dearing,[2] I.W. Croudace,[5] J. Brown[1] and J. Bradley[1]
[1] School of Environmental Science, Liverpool University, UK
[2] School of Geography and Environmental Science, University of Southampton, UK
[3] Department of Geography, Durham University, UK
[4] Department of Geography, King's College London, UK
[5] GAU-Radioanalytical Laboratories, University of Southampton National Oceanography Centre, UK

*Correspondence to: R.C. Chiverrell, School of Environmental Science, Liverpool University, UK. E-mail: rchiv@liv.ac.uk

ESPL

Earth Surface Processes and Landforms

ABSTRACT: We present the first quantitative reconstruction of palaeofloods using lake sediments for the UK and show that for a large catchment in NW England the cluster of devastating floods from 1990 to present is without precedent in this 558-year palaeo-record. Our approach augments conventional flood magnitude and frequency (FMF) analyses with continuous lake sedimentary data to provide a longer-term perspective on flood magnitude recurrence probabilities. The 2009 flood, the largest in >558 years, had a recurrence interval larger (1:2,200 year) than revealed by conventional flood estimation using shorter duration gauged single station records (1:1,700 year). Flood-rich periods are non-stationary in their correlation with climate indices, but the 1990-2018 cluster is associated with warmer Northern Hemisphere Temperatures and positive Atlantic Multidecadal Oscillation. Monitored records rarely capture the largest floods and our palaeoflood series shows, for this catchment, such omissions undermine evaluations of future risk. Our approach provides an exemplar of how to derive centennial palaeoflood reconstructions from lakes coupled well with their catchments around the world. © 2019 The Authors. Earth Surface Processes and Landforms Published by John Wiley & Sons Ltd.

Introduction

Extreme flooding is the world's most damaging natural hazard affecting >100 million people each year (Di Baldassarre *et al.,* 2013; Guha-Sapir *et al.,* 2014). Simulations of 21st century climate change project for many regions an increase in the frequency of occurrence of threatening floods, which currently cost the global community approximately US$1 trillion per year (Hallegatte *et al.,* 2013; Guha-Sapir *et al.,* 2014). A challenge for flood hazard managers and the insurance industry is to identify accurately the magnitude and risk of flooding to develop adequate protection. Flood magnitude and frequency (FMF) analyses are used by industry to estimate the magnitude (design specification for flood protection) and risk (probability of recurrence) of floods. Typically short duration (<50 years) gauging station data underpin most FMF analyses, either directly for single stations or by pooling station series with data from other gauged stations, but neither approach presents a full picture of past flooding (Wilhelm *et al.,* 2013; Macdonald *et al.,* 2014; Wilhelm *et al.,* 2018a; Wilhelm *et al.,* 2018b).

Incorporating additional extreme events from historical or palaeoflood archives can extend the temporal range of FMF analysis (Wilhelm *et al.,* 2018a; Evin *et al.,* 2019) if information on both event timing and magnitude can be secured.

Under the right circumstances, essentially basins well coupled to their catchments, discrete coarser sediment layers record past floods in the sedimentary records of lakes. To date sedimentary palaeoflood analyses have focused typically on event timing with limited estimation of event magnitude (e.g. Schillereff *et al.,* 2014; Wilhelm *et al.,* 2018a; Wilhelm *et al.,* 2018b). Whilst flood frequency data are useful for exploring the relationship between flood phasing and other climate indices (Schulte *et al.,* 2015; Schillereff *et al.,* 2016; Wilhelm *et al.,* 2018a; Wilhelm *et al.,* 2018b) without quantification of event magnitude it is challenging to calculate reliable recurrence intervals (NERC, 1999). Here, we report the first lacustrine palaeoflood record series for a large catchment in the UK and one of few applications of quantitative FMF analyses to sedimentary palaeoflood data (Evin *et al.,* 2019).

Study Site and Methodology

Bassenthwaite lake

Bassenthwaite Lake, NW England (Figure 1A), operates as a large (5.1 km^2) sediment sink receiving drainage and trapping sediments from more than 15% of the upland Lake District National Park (Thackeray *et al.,* 2010). Bassenthwaite Lake is relatively shallow (maximum 20 m and average 5.3 m) and the major inflow rivers enter the south of the lake from the Derwent (254 km^2) and Newlands (49 km^2) catchments. These flows cross a shallow (< 3 m) low gradient littoral zone before descending to a profundal basin that is 200 m wide, 0.5 km from the inflows, 10-12 m deep, and has a pronounced 2-3 m high lip before descent to the deeper basin (19 m) that dominates the remainder of the lake (Figure 1B) (Thackeray *et al.,* 2010). The large catchment, high catchment relief (maximum elevation 950 m) and catchment-to-lake ratio (57:1) combine with average annual precipitation ~2,077 mm to produce a 19-day average water retention time (Thackeray *et al.,* 2010) and conditions ideal for preserving regional palaeoflood data. These conditions are a strong coupling between catchment and lake, a large catchment-to-lake area ratio, a relative simple lake basin geometry that reduces potential for remobilisation, abundant sediment in the catchment and stability to the configuration of inflow streams (Schillereff *et al.,* 2014). Skiddaw Group silt/mudstones to the north and Borrowdale Volcanic Group (andesitic lava and tuff) series to the south form the catchment bedrock. The catchment landscape reflects the impacts of repeated glaciation resulting in steep slopes mantled with glacial debris, both in situ glacial sediments and those modified by periglacial activity. The regional bedrock has been subject to two phases of mineralization producing substantial quantities of metal ore, with a Lower Devonian (Caledonian) age 'chalcopyrite-pyrite-arsenopyrite' phase and early Carboniferous 'galena sphalerite' phase (Stanley and Vaughan, 1982). The catchment was mined for metals (Cu, Zn, Pb, Ba and Co) from the 1560s at numerous locations (Figure 1A), with mining ceasing in the 1970s at Force Crag in the Bassenthwaite catchment (Tyler, 2003; Tyler, 2005a; Tyler, 2005b).

There are lakes upstream of Bassenthwaite Lake that form sediment traps for 120.1 km^2 of the catchment (Figure 1A). The extensive pre-lake floodplain also moderates the downstream flux of sediments, but also is a source of sediment during floods from bank erosion. The dominant wind direction is towards the delta zone and so negates the effects of wind-driven re-suspension to our core sites (Thackeray *et al.,* 2010). The cores were sampled from up-fetch of theoretically modelled regions of wind driven re-suspension in the lake (Schillereff *et al.,* 2014). Boat generated suspended sediment is absent as boating is banned from the southern half of the lake. Thus, the overwhelmingly dominant sediment trajectories to the core site are via river inflows from the River Derwent and Newlands Beck catchments (Johnson and Warburton, 2006; Warburton, 2010).

The Bassenthwaite catchment has experienced a series of recent extreme floods, 2005, 2009 and 2015, with each of these associated with warm, moist south-westerly airstreams and with deep Atlantic depressions tracking north-eastwards across the UK (Barker *et al.,* 2016; Parry *et al.,* 2016). During the largest event from 4 to 6 December 2015, NW England was hit by exceptional and record-breaking precipitation (Storm Desmond) in the Derwent catchment headwaters. The event set new records for 24 hour rainfall totals e.g. Honister Pass 341.4 mm and 322.6 mm at Thirlmere, with rainfall frequency models estimating a local return period of about 1300 years, a 0.08% annual probability (Barker *et al.,* 2016; Burt *et al.,* 2016; Parry *et al.,* 2016). Flood levels for the River Derwent at Portinscale evidence a high magnitude event (365 m^3 s^{-1}), impacting catastrophically on the population and infrastructure.

In November 2009, a weather front became stationary over Cumbria, resulting in prolonged (36 hour) and heavy rainfall (Miller *et al.,* 2013). High altitude areas received more than 400 mm of rainfall (72-hours), setting a then 24 hour rainfall record for the UK in the Bassenthwaite catchment (316 mm, Recurrence Interval ~1,862 years) (Stewart *et al.,* 2012). The resulting peak flow into Bassenthwaite was estimated as 402 m^3 s^{-1} for the River Derwent, with a single-site return period of 228 years (95% confidence limit of >40 and <50,000) (Miller *et al.,* 2013; Wong *et al.,* 2015). At the lake outflow (Derwent at Ouse Bridge: UK Environment Agency), discharge
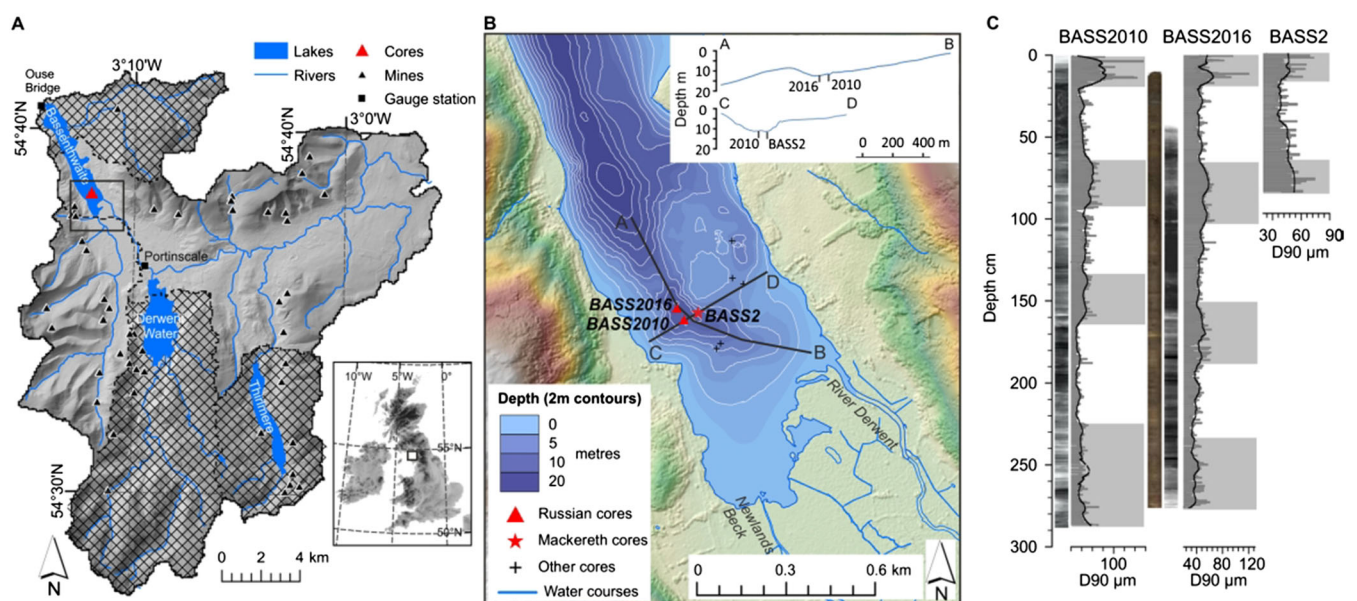
Figure 1. A. Location of Bassenthwaite Lake; the core sites, river gauging stations, metal mines and the active and passive (hatched) sediment supply sectors. B. Core locations, bathymetry and topographical cross-sections (20x vertical exaggeration). C. Line-scan photographs, X-radiographs and 90th percentile (D90) of the PSD data for the three cores (grey: raw D90 data, black: D90 smoothed 25-period centrally weighted function). [Colour figure can be viewed at wileyonlinelibrary.com]

was estimated at 378 m^3 s^{-1} with a single-site return period of 311 (95% confidence limits of >50 <50,000) years (Miller et al., 2013). In January 2005 a westerly airstream generated a near stationary weather front across northern England and southern Scotland that contributed heavy rainfall (<180.4 mm) across Cumbria with an estimated return frequency of <200 years (Stewart et al., 2012) resulting in an estimated peak flow of 219 m^3 s^{-1} on the Derwent (Portinscale) (Miller et al., 2013).

In summary, the river discharges recorded over 40 years for the Derwent at Portinscale show the most three extreme events in the last two decades. These floods have resulted in economic damages totalling £276 million in 2009, and £1.6 billion in 2015 (Storm Desmond) (Environment Agency, 2018) loss of life, extensive flooding of property, the destruction and disruption of infrastructure and the largest river channel adjustments on record (Miller et al., 2013, Wong et al., 2015).

Field and Laboratory Sampling

Sediment cores (BASS-2, BASS-2010 and BASS-2016) came from multiple adjacent sites in the gentle gradient profundal basin that fronts both the Derwent and Newlands river inflows to Bassenthwaite Lake (Figure 1B). The basin has flanking slopes at less than 1-2°, which produces minimal potential for debris flows, wave resuspension and sediment remobilization. BASS-2 (0.8 m: Figure 1C) was sampled collecting the sediment water interface using a piston mini-corer and a gravity corer. Longer sediment records at BASS-2010 and BASS-2016 (both ~2.8 m; Figure 1C) were taken from a stable floating platform and comprise overlapped 1.5 × 0.07 m core lengths and the intact sediment water interface by gravity corer (Boyle, 1995). BASS-2 and BASS-2010 locations (originally sampled 2010) after the November 2009 flood were revisited after the winter storms of 2015/16 (e.g. Storm Desmond) to collect gravity cores and extend the temporal record. Extrusion at 5 mm contiguous intervals produced subsamples from the majority of our piston and gravity cores, with the recent cores after Storm Desmond (December 2015) sampled at 2.5 mm contiguous intervals to characterise better this most recent extreme flood and the preceding flood lamination from November 2009. The stratigraphy in the Russian-style cores is largely uniform in colour comprising grey-brown limnic muds, whereas x-radiographs (BASS-2010, BASS-2016) reveal some finer than 5 mm laminations that reflect subtle variations in sediment density (Figure 1C). Given the lack of a consistent and clear visual stratigraphy (Figure 1C); the palaeoflood records for the sediments were generated using the particle size statistics measured by laser granulometry on the subsamples.

Particle Size and Geochemical Analyses

Sediment geochemistry was determined via X-ray fluorescence (XRF) using two approaches. BASS-2 and all gravity cores were measured using 2.5-5 mm interval discrete samples on a dry-mass basis using a Bruker S2 Ranger energy-dispersive instrument (Boyle et al., 2015; Schillereff et al., 2015). The BASS-2010 and BASS-2016 cores were cleaned, with the BASS-2016 core photographed at 15 µm resolution using the Line-scan camera fitted to the Liverpool Geotek Multi-sensor Core Logger (MSCL) (Figure 1C). Both cores were covered with 5 µm polypropylene film and measured at 5 mm intervals on a wet sediment basis using an Olympus Delta energy dispersive µXRF mounted on the Liverpool Geotek MSCL (Boyle et al., 2015, Schillereff et al., 2015). They were also measured on the Itrax-Core scanner (BOSCORF, National Oceanography Centre, Southampton) using a step size of 300 µm and a measurement dwell time of 30 seconds. A 22 mm wide radiographic image was also collected using the Itrax-CS as a digital, continuous-strip down the core for both BASS-2010 and BASS-2016 (Figure 1C). Wet sediment element concentrations were converted to dry-weight equivalent using a training set of dried samples measured on the S2 Ranger (Boyle et al., 2015). The XRFs undergo regular laboratory consistency checks using certified reference materials (e.g. Boyle et al., 2015).

The palaeoflood record was generated using particle size data measured by laser granulometry, given the strong sediment hydrodynamic relationship with river discharge (see reviews in Schillereff et al., 2014, Wilhelm et al., 2018b) and also the patchy visual signature for the coarse grained units at Bassenthwaite (Figure 1C). Analysis using a Coulter LS 13 320 Single-Wavelength Laser Diffraction Particle Size Analyser, which determines the dimensions of individual particles 0.375-2000 µm, measured particle size distributions (PSD) for the subsamples. Digestion in H$_2$O$_2$ removed the organic component, with the samples then dispersed and sonicated in Na$_6$O$_{18}$P$_6$ and analysed under sonicating measurement conditions. Results are the average of three repeats after elimination of outliers, a process that minimises intra-sample noise in the laser granulometry. The Coulter LS 13 320 undergoes regular calibration checks using samples with known size distributions. Particle size frequency statistics were calculated using standard geometric formulae (Folk and Ward, 1957) using the GRADISTAT 8.0 software (Blott and Pye, 2001). Further data exploration involved a statistical end-member analysis using the EMMAgeo package (Dietze and Dietze, 2016) to identify and quantify the proportions of significant PSD end members (EM) using a principal components methodology implemented in R (R Core Team, 2017).

Geochronology

Sediment core chronologies were generated by Bayesian age-depth modelling (Blaauw and Christen, 2011) of radioisotope dating (^{210}Pb, ^{137}Cs and ^{14}C) and using a metals geochemical stratigraphy (Pb, Zn, Ba and Cu) that reflects the catchment history of mineral ore production. Generating robust chronological control for sediment sequences spanning the last 500 years is difficult and compounded by significant changes in sedimentation rate (SR) rendering ^{210}Pb dating (Appleby and Oldfield, 1978; Appleby, 2008; Appleby, 2013) challenging. However, the rich record of historical (CE 1560-1950) metal pollution for the Bassenthwaite catchment (Figure 2B) provides data for an age-depth model generated for the lake sediments (Tyler, 2003; Tyler, 2005a; Tyler, 2005b). We recovered repeatable geochemical records for the metals Cu, Pb, Zn, and Ba from multiple core sites (Figure 2C) and these data show a strong match to the history of metal ore production collated for mines in the active catchment (Figure 2B) (Tyler, 2003, Tyler, 2005a, Tyler, 2005b). Coherence of the inflow-derived metal stratigraphic record supports the lack of major resuspension of sediments by wind driven stress in this region of the lake (Thackeray et al., 2010; Schillereff et al., 2014). From the metals data (Figure 2C: repeatable across these three and other cores) a series of chronological marker horizons (Table I) were identified for the sediments spanning the last 400 years. Pb concentrations have been plotted against both linear and log axes for BASS-2010 and BASS-2016, because the high concentrations from CE 1800 dwarf smaller in magnitude patterns in the earlier record (Figure 2C).
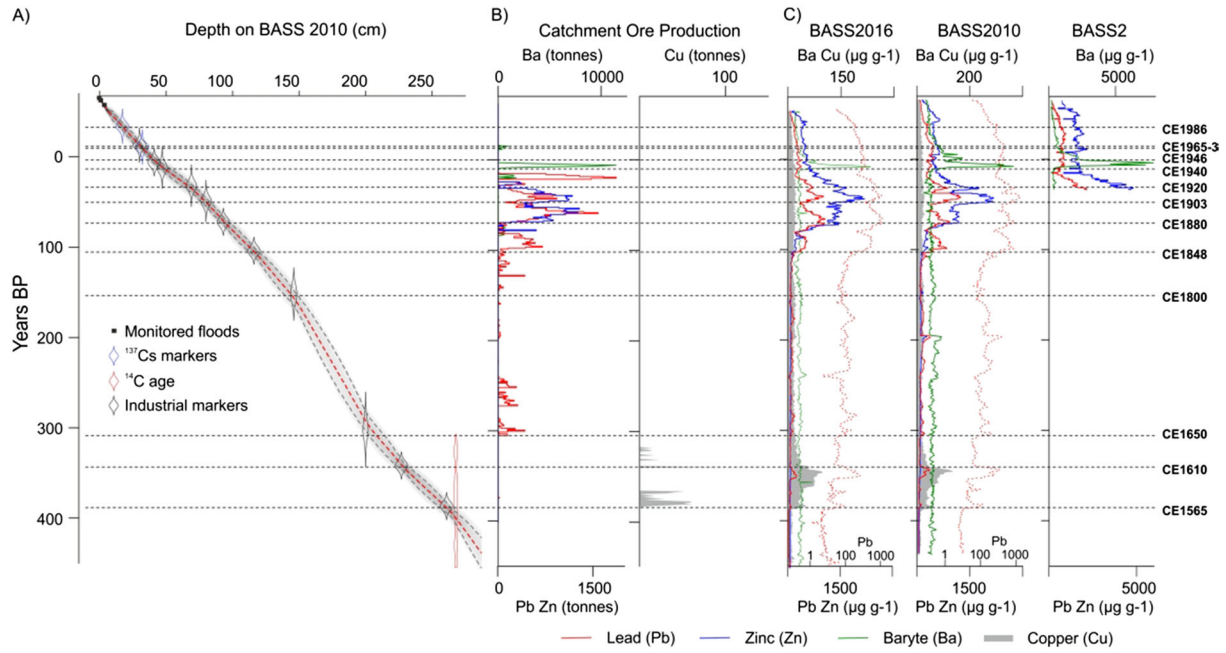
Figure 2. Age-depth information for Bassenthwaite Lake and the metal pollutant stratigraphy. A. Geochronological data and the Bayesian age-depth model for BASS-2010 showing the pollution markers, a ^{14}C age, markers for fallout radionuclides (^{137}Cs) in 1963 and 1986, the modelled weighted mean age (red pecked line), the 2 σ age probability (greyscale), and 2 σ uncertainty age range (grey pecked lines). B. Metal ore production in tons from mines in the catchment (Tyler, 2003; Tyler, 2005a; Tyler, 2005b). C. Metal concentration data measured by XRF plotted against age derived from age-depth models for BASS-2016, BASS-2010 and BASS-2. Pb (solid red), Zn (blue), Ba (green) and Cu (grey fill). Pb is plotted for BASS-2016 and BASS-2010 with a log axis (red dashed line) to show patterns at lower concentrations. Time markers and their age extend across the plot (see Table I). [Colour figure can be viewed at wileyonlinelibrary.com]

Radiometric dating, using [137]Cs (half-life of 30 yr) and [210]Pb (half-life of 22.4 yr) was carried out for BASS-2 using established methods (Croudace et al., 2012; Miller et al., 2014; Sjögren et al., 2017) at the GAU-Radioanalytical Laboratories (National Oceanography Centre, Southampton). Bulk dried and homogenised samples were counted for 100,000-seconds in scintillation vials using Canberra well-type HPGe spectrometers (Canberra Industries, Harwell, UK). Gamma spectra were processed using FITZPEAKS gamma deconvolving software (JF Computing, Stanford in the Vale, UK). The photo-peak areas for [210]Pb (46 keV), [137]Cs (661 keV) and other

gamma radionuclides were calibrated using a certified NPL radionuclide mixture dispersed in a sediment matrix. Detection limits are nominally 5 Bg/kg for ^{210}Pb and 2 Bq/kg for [137]Cs. The ^{210}Pb activity vs depth profile (Figure 3A) shows a general exponential form implying a uniform sediment rate for the sequence down to approximately 40 cm depth, below which patterns in the measured 210 PB concentrations make age estimation unreliable. The anthropogenic radionuclide ^{137}Cs profile for Bass2 (Figure 3B) shows two key datable features: the CE 1963 'main bomb pulse' [137]Cs from atmospheric nuclear testing and the CE 1986 Chernobyl spike. These features

Table I. Age depth information for the BASS-2, BASS-2010 and BASS-2016 sediment profiles

Event marker or dating information	Calendar Age	Years BP	Radiometric age	Age Uncertainty	Depth in core		
					BASS2016	BASS2010	BASS2
Sediment surface	2016	-66	-	1	0	0	0
Monitored storm layer 2015	2015	-65	-	1	1	1	1
Monitored storm layer 2009	2009	-59	-	1	3	3	2.8
Chenobyl 137Cs peak	1986	-36	-	4	24*	17	31
End in production at Force Crag Mine	1965	-15	-	4	35	30	40
Weapons testing 137Cs peak	1963	-13	-	4	37*	32	42
Decline in Ba production at Force Crag Mine	1946	4	-	5	48	41	52
Onset of Ba at Force Crag Mine	1940	10	-	5	56	47	60
Pb/Zn coproduction Goldscope - Threkeld Mines	1920	30	-	5	73	69	86
Pb/Zn coproduction Goldscope - Threkeld Mines	1903	47	-	5	82	80	-
Pb/Zn coproduction Goldscope - Threkeld Mines	1880	70	-	5	99	93	-
Increase in Pb production - Goldscope Mine	1848	102	-	5	113	116	-
Early Pb production at Goldscope Mine - Phase 2	1800	150	-	10	144	146	-
Early Pb production at Goldscope Mine - Phase 1	1650	300	-	10	184	200	-
Cessation of Cu at Goldscape Mine	1610	340	-	5	199	227	-
16th century Cu at Goldscope Mine	1565	385	-	5	224	261	-
14C age (SUERC-41877)	-	-	329	24	229*	268	-

*= equivalent depth
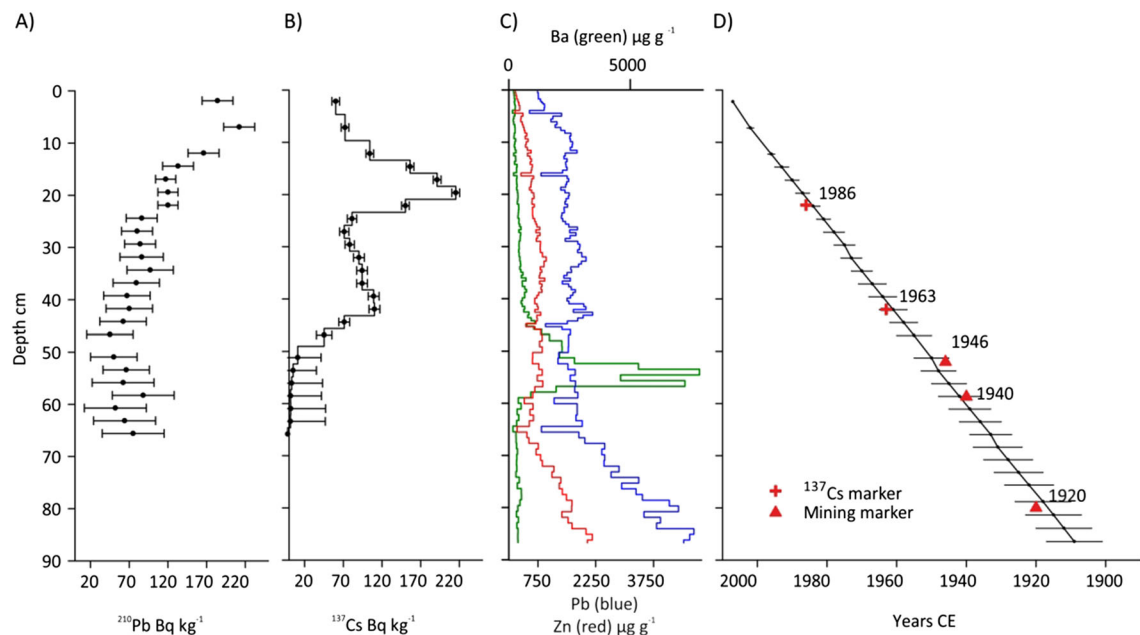
Figure 3. Age depth information for BASS-2 showing: A) supported ^{210}Pb records, B) 137Cs records, C) dry mass elements concentrations of Pb, Zn and Ba measured by XRF, D) ^{210}Pb age-depth model compared with mining and artificial radionuclide (^{137}Cs) markers. [Colour figure can be viewed at wileyonlinelibrary.com]

identify an average sedimentation rate of 0.87 cm/y. A linear regression of the Ln^{210}Pb data (less a supported ^{210}Pb of 10 Bq/kg; Simple Model) gives a sedimentation rate of 0.90 cm/y which is consistent with the average from ^{137}Cs dating (Figure 3D). The markers for mined heavy metals and ^{137}Cs horizons (Figure 3C-D) incorporated and show a strong fit to the independent ^{210}Pb radioisotope chronology (Figure 3). The single ^{14}C age determination of 329 ± 24 BP (SUERC-41877) from a terrestrial leaf fragment at 2.68 m depth on BASS-2010 is a good fit to the longer metals stratigraphy (Figure 2A).

The final age models were produced independently for each core profile, using all the geochronological control using the Bayesian package 'rBacon'(Blaauw and Christen, 2011; Blaauw and Andres Christen, 2018) operating in R (R Core Team, 2017). Markov Chain Monte Carlo repetitions in the age-depth modelling were constrained by a gamma distribution with mean 2 yr mm^{-1} and shape 1.5 and a beta distribution with mean 0.4 and memory strength 25. The lack of a consistently clear visual stratigraphy for the core negated the incorporation of geologically instantaneous event laminations in the age-depth model. Sedimentation rates throughout the profile average 6 mm yr^{-1}, and vary from to 4-10 mm yr^{-1} with the exception of the high water content surface sediments. Thus the 5 mm contiguous sampling implicit in the PSD analyses are close to an annual resolution. The timing of events discerned in the palaeoflood series uses the probability weighted mean age and 95% uncertainties from the Bayesian age-depth model (Figure 2A).

Developing the Sedimentary Palaeoflood Record`

The age-depth model displays a series of variations in SR (Figure 4C) and these are largely mirrored in increased flux of lithogenic elements (e.g. K: Figure 4C), and these are interpreted as responses to catchment soil/sediment erosion conditioned mostly by agricultural intensification and a minor contribution from metal mining. Timescales for patterns present in regional palaeo-vegetation data (Pennington, 1981; Pennington, 1991; Chiverrell, 2006) support linkage of these

erosion phases to agricultural intensification. The PSDs (Figure 4) show repeated and regular laminations that contain a coarser component. End-Member (EM) analyses (Dietze *et al.,* 2012) for an integrated dataset from the cores decomposes the PSDs into two groupings that explain 87% of the variance in the dataset (Figure 4F). EM1 comprises fine silt (7 -8 μm), whereas EM2 is coarser and comprises a fine sand (mode = 63 μm). Where present EM2 forms more than 30% of the PSD and occurs as discrete laminations or beds (Figure 4B). The 90th percentile of the PSDs (D90) is a strong measure of this coarse EM2 and characterises the falling limb of the distributions. Our process interpretations for the end members is that EM1 reflect background or normal accumulation of fine grained gyttja and the EM2 coarser deposits lain down under flood conditions. The absence of further statistically significant PSDs end members, we interpret as reflecting that other process end members are not a component of the Bassenthwaite Lake record. At other deeper British lakes, with steeper gradient lake beds, we have encountered multimodal poorly sorted PSDs as layers, which are probably subaqueous debris flows and have characteristics similar to equivalent deposits in other environments (Håkanson and Jansson, 1983; Mulder and Alexander, 2001). Peaks in the D90 and EM2 form repeated sub-centimetre coarser laminations that display poor sorting and right-skewed distributions. Lower-frequency down core changes in EM2 and the D90 show the sediments are coarser grained when there are increases in the SR and/or the flux of lithogenic elements (Figure 4C), e.g. K which is abundant in the catchment bedrock, sediments and soils. These changes reflect subtle variations in sediment availability to the fluvial system, typically driven in the longer term by patterns of land use change and high magnitude erosion events enriching the channel system with coarser sediment. The smoothed D90 curve describes these changes in the baseline grain size regime and they are subtle varying in the range 60-40 μm (Figure 4D). Coarse laminations dominated by EM2 punctuate the smoothed record with the increases in D90 much larger than the background variations. These coarse laminations are present throughout the record therefore the inflow channels and pre-lake floodplain appears to have provided abundant sediment to Bassenthwaite Lake (Orr *et al.,* 2004; Warburton, 2010).
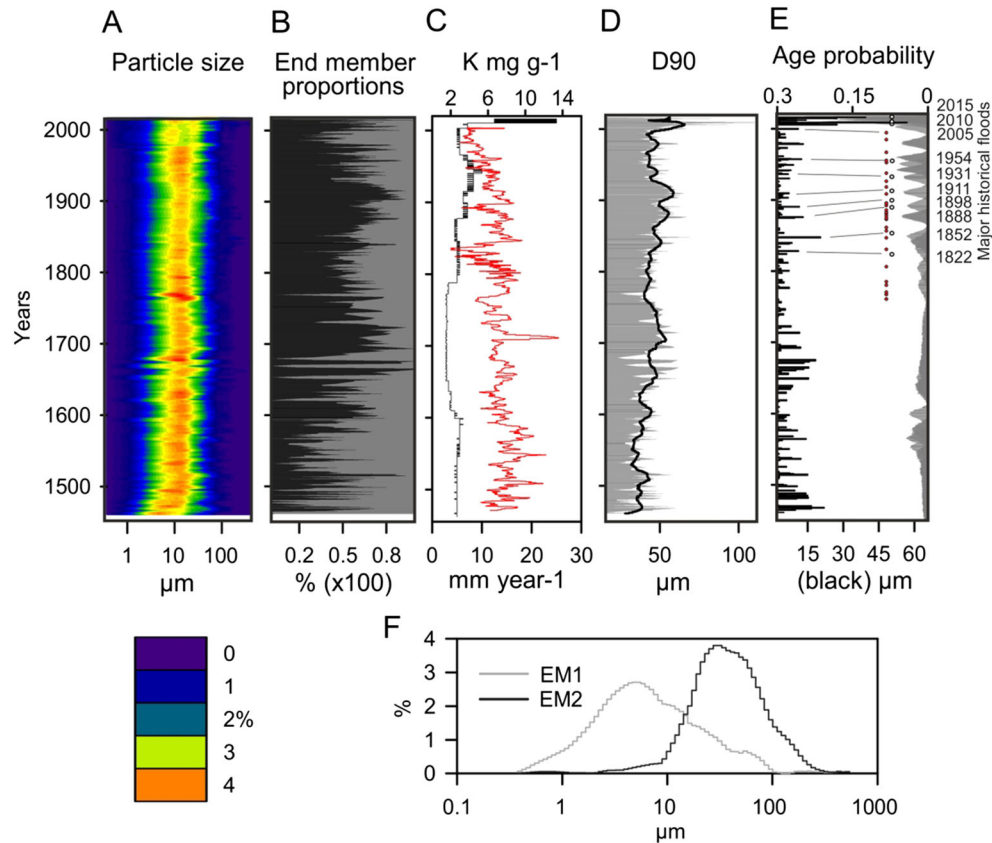
Figure 4. For BASS-2016, A. 3-dimensional colour contour plot of volume percent PSD. B. Proportions of the particle size distributions of end members EM1 and EM2. C. Sedimentation rates (SR) mm year^{-1} and K concentrations measured by XRF (mg g^{-1}). D. 90th percentile (D90; grey) of the PSDs fitted with a 25-period centrally weighted smoothing function (D90smoothed; black). E. The positive D90 residuals (black line: D90 minus D90smoothed) and 2 σ age probabilities for flood layers (>115 m^3 s^{-1}) showing major and minor floods from the Chronology of British Hydrological Events entries for the Derwent/Cocker catchment (http://www.cbhe.hydrology.org.uk/) (Black and Law, 2004). F. PSDs of the statistically significant particle size end members. [Colour figure can be viewed at wileyonlinelibrary.com]

Changes in the D90 smoothed baseline suggest that the catchment sedimentary regime is not stationary. To correct for this we calculated i) a centrally weighted 25-point (~125 mm) smoothing function (D90smoothed) and ii) the residuals of D90 against D90smoothed. This D90residual expresses the PSDs in terms of their magnitude (μm) within a 40 year moving temporal window that is similar in length to gauged recorded river flow records (Miller *et al.*, 2013). We undertook a sensitivity analysis of the effect of our sampling resolution on this D90residual. Samples were taken at 2.5 mm resolution over the period containing the most recent known extreme floods (2009-2016) and measured for PSD. The PSD were then combined to intervals equating to 5, 10, 15 and 20 mm contiguous sampling, and the D90residuals were recalculated. The resulting variance across known discrete extreme events was ~5%. Applying this variance to the entire palaeoflood dataset suggests our sampling resolution has no impact on the estimation of relative magnitudes for extreme events.

We are cautious about allocating specific flood layers to historical documented floods; rather we assign each sedimentary flood a ±2σ age range derived from the Bayesian age-depth models (Figure 2A). The precise event lamination is regarded therefore as constrained to a defined period within which historic floods may fall. BASS-2016 extends the duration of this palaeoflood record and shows cluster of events at 1840-1925 and 1930-2016 (Figure 4E) that match flood-rich periods in both the regional and local historical data (Black and Law, 2004; Macdonald and Sangster, 2017). The magnitude of the largest floods, 12/2015 (364 m^3 s^{-1}), 11/2009 (402 m^3 s^{-1}), 8/2005 (219 m^3 s^{-1}) and 1/1995 (159.6 m^3 s^{-1}) (Derwent at

Portinscale), broadly matches the magnitude ranking in the D90residual (Figure 5). We are therefore confident that our reconstructed palaeoflood series from lake sediments is recording the structure and individual flood hydrology of the catchment. Extending the flood record back to 1460 reveals distinct earlier flood-rich phases (c.1460-1575, c.1630-1720), which are concomitant with events present in historical datasets for northwest England (Macdonald and Sangster, 2017).

For the past 43 years the sediment flood record shows a significant correlation (r^2 = 89%) with a gauged discharge (m^3 s^{-1}) flood series for the Derwent (Portinscale) (Figures 5C). To generate a training data set for flood frequency analysis (FMF) including assessment of flood magnitude we allocated peaks in the D90residual from the recent gauged period (1970-2018) to flood discharges (Figure 5). The gauged period contains a range of floods including four recent extreme events. Best-fit regression was used to define an exponential function (r^2 = 89%, p<0.0001) describing the relationship between recorded discharges and D90residual (Figure 5C). Applying this function to the entire D90residual time series produced a sedimentary palaeo-discharge series (Figure 6A). The precision of the reconstructed discharges are +/- the uncertainty inherent the exponential function as with any model, but we are confident in the relative magnitudes that are important for using the time series in subsequent FMF. To assess the impact of calculating the D90residual as a palaeoflood proxy, an equivalent best fit (linear) regression model was generated for the relationship between recorded discharges and raw D90 (r^2 = 70%, p<0.0001), and the application of that to the entire D90 time series is virtually identical to the discharge reconstruction using the D90residuals. Thus, whilst there is some non-
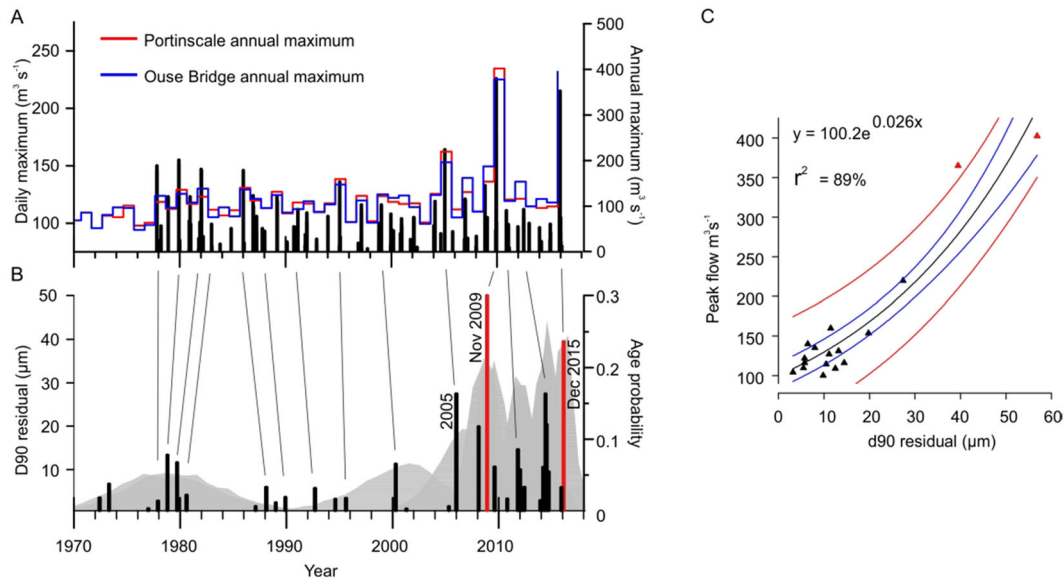
Figure 5. A. Gauged annual maximum (AMAX) river discharges at Portinscale (red line) and Ouse Bridge (blue line) gauging stations, alongside daily maximum flow data from Portinscale (black bars) all in m^3 s^{-1}. B. D90residual (µm) (black bars) and 2 σ age probabilities (grey) for sedimentary flood layers. C. Relationship between D90residual (µm) and the equivalent gauged peak river flow (m^3 s^{-1}) for the given year at Portinscale. Shown with 1 sigma (blue) and 2 sigma (red) uncertainties. [Colour figure can be viewed at wileyonlinelibrary.com]
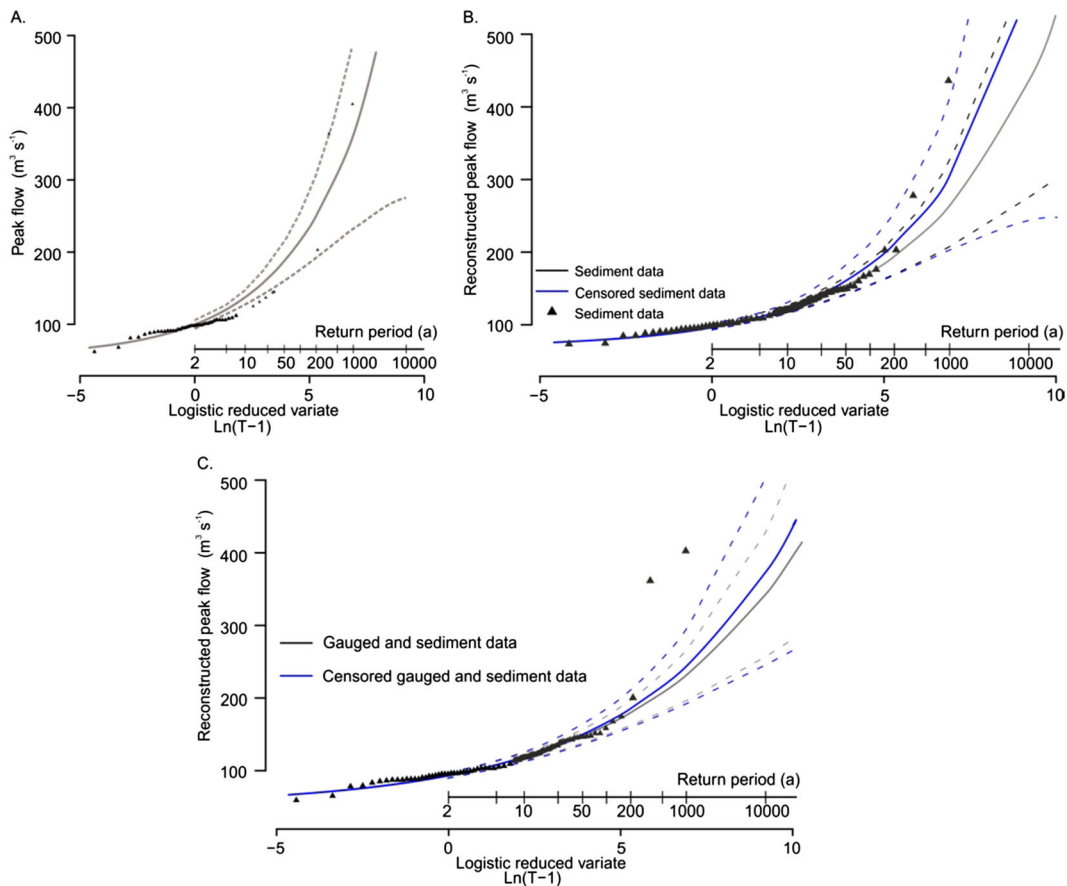
Figure 6. A. Flood magnitude frequency (FMF) analysis with recurrence intervals showing 95% uncertainties (pecked lines) for Portinscale single site gauged discharge data only. B. Modelled FMF analysis recurrence intervals showing 95% uncertainties (pecked lines) for palaeoflood reconstructed discharges at BASS-2016, using both (i) the entire reconstructed sedimentary series (black) and (ii) a peaks-over-threshold (>115 m^3 s^{-1}) series derived from the sedimentary series (blue). C. Modelled FMF analysis with recurrence intervals showing 95% uncertainties (pecked lines) for (i) the gauged series (CE 2018-1970) augmented by palaeoflood reconstructed discharges for the period CE 1970-1490 (grey) and (ii) the same data expressed as peaks-over-threshold (>115 m^3 s^{-1}; blue). For A-C the contributing gauged and reconstructed river flow data are shown plotted (triangles) against a logistic reduced variate axis. [Colour figure can be viewed at wileyonlinelibrary.com]

stationarity due to changes in catchment state arising from agricultural land-use intensity; it appears to have little or no impact on the grain sizes delivered to Bassenthwaite Lake in flood

events over the last 558 years. Detrending the flood series has no negative impacts on the flood series, for example, there is no exaggeration of the extremes of the past two decades, with

the extreme peaks reducing in magnitude in the calculation of the D90residual.

Flood Magnitude Frequency (Fmf) Analysis

Here we explore the impact of including the palaeoflood series in FMF analyses, with the analysis involving fitting of a Generalised Logistic (GLO) distribution to the reconstructed series of peak flow events ($m^3 s^{-1}$) based on the method of L-moments (Robson and Reed, 1999; Castellarin et al., 2012). The logistic reduced variate generated permits the cumulative probability distribution to be plotted in linear relationship to the discharge, assuming a logistic (no skewness) distribution. No conclusive method has been developed within the L-moment framework for combining gauged data with censored (either historical or sedimentary) events in the period pre-dating the installation of a gauging station. A probabilistic model (Macdonald et al., 2014) has been proposed for censored annual maximum series formulated as a maximum-likelihood function (NERC, 1999). This model assumes that events from the gauged and historical/sedimentary period are independent and follow a GLO distribution with a Probability Density Function (PDF) and Cumulative Density Function (CDF).

The FMF analyses drew upon four flood time series:

1. a single station (Portinscale) gauged series 2016 to 1970 (Figure 5A),
2. the sedimentary proxy discharge data for BASS-2016 (Figure 6A),
3. the sedimentary series expressed as Peaks Over Threshold (POT) with events <115 $m^3 s^{-1}$ excluded (Macdonald et al., 2014), and
4. the gauged series 2016 to 1970 augmented by the sedimentary series from CE 1970 to 1460 with events <115 $m^3 s^{-1}$ excluded.

The 115 $m^3 s^{-1}$ threshold was identified to ensure a similar number of high magnitude floods were included in both the gauged and sedimentary data series, and was based on no two events within any given year in either the sedimentary or instrumental series exceeding the >115 $m^3 s^{-1}$ threshold (Macdonald et al., 2014). Using a high threshold ensures that it can be reasonably concluded that the two data series (gauged and sedimentary) are both realizations of the same underlying distribution (Macdonald and Sangster, 2017).

Confidence intervals for the different flood frequency curves are presented (Figure 6A-C), using the Delta method adopted to obtain a confidence interval for a given annual threshold event (e.g. 1 in 100 or 1 in 1,000 years) (as shown in Kjeldsen and Jones, 2006). The fitted GLO models (Figure 6B) are plotted with 95% confidence intervals against the observed AMAX showing: the GLO distribution fitted directly to the 43 annual maximum events in the gauged record (Gringorten plotting position); and the GLO distribution fitted to the sedimentary data series (for assumptions of known and unknown peak discharges) (Macdonald et al., 2014). In applying a censored approach (>115$m^3 s^{-1}$; Figure 6B-C) the censored sedimentary series is statistically treated as Peak-Over-Threshold (POT) data (Macdonald et al., 2014). These differing series highlight an important difference between 1) water dominated floods reflected in gauged records and 2) the sediment dominated floods implicit to the lake palaeorecord. More often than not for the larger floods water and sediment dominated overlap, but in identifying event magnitude from the sediments then we are

also capturing the importance of sediment supply in the flood event, which is an aspect not present in the gauged record.

The single site (gauged) FMF analysis (Figure 6A) compares well with previously published FMF analysis at Camerton, further downstream in the Derwent catchment, with single site and a data pooling approach used (Miller et al., 2013). Pooling is a conventional approach in flood frequency estimation used when a single discharge series is of insufficient length in determining a required estimate for a design flood (Robson and Reed, 1999). Pooled FMF categorized the November 2009 flood as the largest on record with a return period of between 50 and 500 years (Miller et al., 2013). Here, our single station FMF analysis using the gauged annual maximum series for Portinscale suggests a return period of 1,700 years for the 2009 flood (Figure 6A). Incorporating the full palaeoflood record into the FMF analysis increases this return period to ~10,000 years reducing to ~2,200 years when the series was censored to the peaks >115 $m^3 s^{-1}$ threshold (Figure 6B). Incorporating our threshold censored palaeoflood data into the FMF analysis reduces the magnitude of the estimated 100- and 1,000-year events compared to that generated using the 43 year gauged series alone, reducing from ~215 to ~182 $m^3 s^{-1}$ and from ~365 to ~300 $m^3 s^{-1}$ respectively (Figure 6B). Our palaeoflood data (Figure 6B) show that ~2,200 year (1,050 to >10,000 years: 95% confidence interval) return period for 2009 flooding was rarer than indicated by the short gauged record (Figure 6A) and the 50-500 year return period calculated in FMF analysis conducted before Storm Desmond for the Derwent (Camerton) using a data pooling approach (see Miller et al., 2013).

FMF analysis using the palaeoflood series returns a ~750 year (300 to >10,000 years) return period for the 2015 flood (Storm Desmond), which is slightly shorter than the 1,000 year (375 to >10,000) indicated by equivalent single station analysis of the Derwent (Portinscale) gauged series (Figure 6A). The discrepancy for the 2015 event reflects the lower discharge reconstructed from the sediment palaeorecord. FMF analysis using the gauged series augmented by sedimentary palaeoflood data applying a censored approach (>115 $m^3 s^{-1}$; Figure 6C), shows the impact of including a further high magnitude event on the analyses. Combining gauged with the sedimentary series produces estimated magnitudes for 100- and 1,000-year events of 170 $m^3 s^{-1}$ and 250 $m^3 s^{-1}$ respectively, and the return periods for the 2009 and 2015 to ~20,000 and ~14,000 years respectively. The sedimentary palaeoflood series reveals that the magnitudes of floods over the last 20-25 years form a cluster without equal and unprecedented in ~558 years (Figure 7A).

Analysis of Climate Indices

Comparing records of past precipitation and associated fluvial flooding to a range of climate and ocean indices can improve our understanding of the forcing of extreme weather. Instrumental and modelled data (Sutton and Dong, 2012; Huntingford et al., 2014) record a relationship between winter (DJF) North Atlantic Oscillation (wNAO) and rainfall over NW England. Positive wNAO indices are associated with higher precipitation and river flows via increased cyclonicity and enhanced zonal flow over the region (Hannaford and Marsh, 2008; Lavers et al., 2011). Since wNAO tends are positively correlated with Mean Annual Temperature, it is likely that the moisture content of westerly air masses will also increase when the wNAO index is strongly positive, amplifying the impact of increased airflow (Hannaford and Marsh, 2008, Lavers et al., 2011). Thus, the effects of warming northern hemisphere
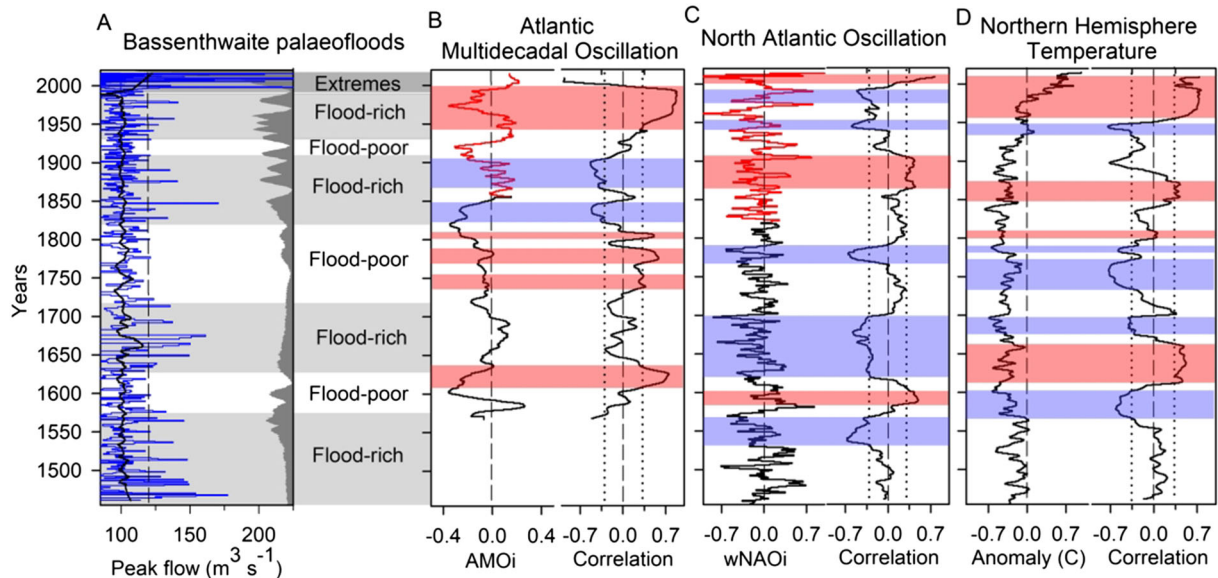
Figure 7. A. Time series of raw (blue) and smoothed (black) river flow series ($m^3\ s^{-1}$) reconstructed from core BASS-2016, showing the modelled age probabilities for flood layers (>115 $m^3\ s^{-1}$), with flood-rich periods and episodes of extreme flooding. B. Indices for Atlantic Multidecadal Oscillation (AMO) (left: measured series in red, reconstructed in black) (Cook *et al.,* 2002) and a Pearson correlation co-efficient series (right) relating the AMO and the smoothed Qmax series. Vertical lines (pecked) show zero correlation and the 99% significance limits. Shaded rectangle zones highlight periods with significant positive (red) and negative (blue) correlation. C. The same as B except for indices of winter North Atlantic Oscillation (wNAO; Gray *et al.,* 2004). D. The same as B except for reconstructed Northern Hemisphere Temperatures (NHT; Shi *et al.,* 2013). [Colour figure can be viewed at wileyonlinelibrary.com]

temperatures (NHT) could potentially increase the moisture content of westerly airflows during positive wNAO. There is observational and modelling evidence of increases in rainfall over NW Europe associated with a positive wNAO index and a switch to a more positive phase of Atlantic Multidecadal Oscillation (AMO) (Sutton and Dong, 2012).

In an attempt to move beyond visual comparison of curves (Figure 7), we have explored the strength of the relationship between our palaeorecord of POT and a series of climate indices linked with the occurrence of storms and river floods in NW Europe (Blöschl *et al.,* 2017). The duration of our POT series extends beyond the measured wNAO and AMO (red lines: Figure 7B, C), and so we have used a composite series (black lines: Figure 7B, C) that is integrated with published longer reconstructed time series. These series were: i) a tree ring based reconstruction of the AMO (Gray *et al.,* 2004) back to 1567 (Figure 7B); ii) a multi-proxy reconstruction of wNAO (Cook *et al.,* 2002) back to 1400 (Figure 7C); and iii) an annually-resolved reconstruction of northern hemisphere temperatures for the last millennium (Shi *et al.,* 2013) from annually-resolved palaeo-data (Figure 7D). Each of these proxy records performs well against the equivalent measured data for a >150 year duration calibration period (Cook *et al.,* 2002; Gray *et al.,* 2004; Shi *et al.,* 2013), and is of sufficient duration for comparison with our POT series that extends to 1460.

There is no significant correlation (Pearson product moment) on a whole record basis for the D90residual or for the D90residual record smoothed with a 40 year moving average with the selected climate indices (Figure 7A). The calculated correlation analyses for a time-stepped 50 year moving window through the datasets highlights periods with significant positive (red) and negative (blue) correlation using 99% significance limits (right panel: Figure 7B-D). Limitations to this analysis stem from comparing the sedimentary palaeoflood series with an average chronological uncertainty of ±18.5 years (2σ range 1.4 to 50.1 years) with annually resolved reconstructions, alongside the uncertainties inherent in the selected reconstructions (Cook *et al.,* 2002, Gray *et al.,* 2004, Shi *et al.,* 2013), and should be viewed in the context that a phase with a significant

correlation does not implicitly mean causation. Thus, we do not attempt a mechanistic interpretation; rather our data (Figure 7B-D) suggest that the relationships between hydroclimatic indices typically associated with flood studies are non-stationary over time. There is no clear and consistent relationship between our palaeoflood series and wNAO. The more flood-rich periods 1460-1570, 1640-1720 and 1820-1910 show some positive correlations with negative wNAOi, warm phase (positive) AMO and warmer NHT. The flood-poor periods 1570-1640, 1720-1820 and 1910-1940 correspond with cooler phase (negative to neutral) AMO. The flood rich period 1940-1990 corresponds with cool phase (negative) AMO, but the shift to warmer NHT. The more extreme winter floods 1990-2018 were only significantly and positively correlated with oscillations in the wNAOi, warm phase (positive) AMO and warmer NHT including >4 of globally the warmest years on record (NOAA, 2018). Extreme flooding 1990-2018 shows a weak relationship with wNAO, which was in a strongly negative mode for the winter floods of 2009 and 2005, but positive for December 2015.

Conclusions

We show the value of lake sediments in extending the flood series used to estimate the probability of high extreme magnitude events. Short flood records and non-stationarity in climate time series can hamper flood design estimation. Our results illustrate that increasing the record length, here using sedimentary palaeoflood data, has lengthened the return period estimates for these events produced by FMF analyses. Reconstructions of flood series have focused less on variability in flood magnitude and more on the phasing of flood-rich and poor periods (Hall *et al.,* 2014). This focus reflects the challenges in reconstructing event magnitude rather than just frequency, and that flood phases rather than individual events are easier to attribute to climatic forcing. UK-scale assessments of recent flooding (Wilby and Quinn, 2013) show that during the last 140 years the recent flood-rich decade is unusual, but not

unprecedented. Our continuous 558-year palaeoflood time series that incorporates both event magnitude and frequency shows that the extreme floods (top 1%) whilst infrequent occur in groups and that the most extreme floods in our series clustered between 1990 and 2018 (Figure 7). Potentially, FMF analyses derived using short gauged time series during a cluster of extremes could produce recurrence probabilities that are too frequent; which might lead to higher estimates of flood risk and costly over-design of flood defences. Thus, being able to identify the longer-term context for the shorter gauged records is critical in helping refine plans for flood protection. Furthermore, our focus on magnitude frequency relationships for palaeofloods targets the geomorphologically important events, and provides an assessment based on the sediment-floods associated with societal flood impact (e.g. erosive floods). Calibrated reconstructions of long-term flood magnitude can also help more accurately parameterize statements about the "unprecedented" nature of floods and long-term data that our approach can yield require reconsideration of the definitions of unprecedented flooding. Our approach is widely applicable at lakes that are well-coupled to the hydrodynamics of their catchments (see reviews in Schillereff *et al.,* 2014; *n*=152 such lakes in UK alone) offering the possibility of quantitative long term flood series for different hydroclimatic regions of the world. Future research should focus on developing such records for other hydroclimatic areas to understand better the drivers and responses to regional variability and extension of records back into periods characterized by warmer NHT such as the Medieval Climatic Optimum.

References

Appleby PG. 2008. Three decades of dating recent sediments by fallout radionuclides: A review. *Holocene* **18**: 83–93.

Appleby PG. 2013. 210Pb dating: Thirty-five years on. *Journal of Paleolimnology* **49**: 697–702.

Appleby PG, Oldfield F. 1978. The calculation of lead-210 dates assuming a constant rate of supply of unsupported 210Pb to the sediment. *Catena* **5**: 1–8.

Barker L, Hannaford J, Parry S. 2016. Briefing note. Severity of the December 2015 floods-preliminary analysis.

Blaauw M, Andres Christen J. 2018. rbacon: Age-Depth Modelling using Bayesian Statistics. In *R package version 2.3.2.*

Blaauw M, Christen JA. 2011. Flexible paleoclimate age-depth models using an autoregressive gamma process. *Bayesian Analysis* **6**: 457–474.

Black AR, Law FM. 2004. Development and utilization of a national web-based chronology of hydrological events/Développement et utilisation sur internet d'une chronologie nationale d'événements hydrologiques. *Hydrological Sciences Journal* **49**. https://doi.org/10.1623/hysj.49.2.237.34835.

Blöschl G, Hall J, Parajka J, Perdigão RAP, Merz B, Arheimer B, Aronica GT, Bilibashi A, Bonacci O, Borga M, Čanjevac I, Castellarin A, Chirico GB, Claps P, Fiala K, Frolova N, Gorbachova L, Gül A, Hannaford J, Harrigan S, Kireeva M, Kiss A, Kjeldsen TR, Kohnová S, Koskela JJ, Ledvinka O, Macdonald N, Mavrova-Guirguinova M, Mediero L, Merz R, Molnar P, Montanari A, Murphy C, Osuch M, Ovcharuk V, Radevski I, Rogger M, Salinas JL, Sauquet E, Šraj M, Szolgay J, Viglione A, Volpi E, Wilson D, Zaimi K, Živković N. 2017. Changing climate shifts timing of European floods. *Science* **357**: 588–590. https://doi.org/10.1126/science.aan2506.

Blott SJ, Pye K. 2001. Gradistat: A grain size distribution and statistics package for the analysis of unconsolidated sediments. *Earth Surface Processes and Landforms* **26**: 1237–1248.

Boyle JF. 1995. A simple closure mechanism for a compact,mlarge-diameter, gravity corer. *Journal of Paleolimnology* **13**: 85–87.

Boyle JF, Chiverrell RC, Schillereff D. 2015. Approaches to water content correction and calibration for µXRF core scanning: comparing X-ray scattering with simple regression of elemental concentrations. In *Micro-XRF Studies of Sediment Cores.* Springer; 373–390.

Burt S, McCarthy M, Kendon M, Hannaford J. 2016. Cumbrian floods, 5/6 December 2015. *Weather* **71**: 36–37. https://doi.org/10.1002/wea.2704.

Castellarin A, Kohnová S, Gaál L, Fleig A, Salinas J, Toumazis A, Kjeldsen T, Macdonald N. 2012. Review of applied-statistical methods for flood-frequency analysis in Europe.

Chiverrell RC. 2006. Past and future perspectives upon landscape instability in Cumbria, northwest England. *Regional Environmental Change* **6**: 101–114. https://doi.org/10.1007/s10113-005-0005-6.

Cook ER, D'Arrigo RD, Mann ME. 2002. A well-verified, multiproxy reconstruction of the winter North Atlantic Oscillation index since AD 1400. *Journal of Climate* **15**: 1754–1764.

Croudace IW, Warwick PE, Morris JE. 2012. Evidence for the preservation of technogenic tritiated organic compounds in an estuarine sedimentary environment. *Environmental Science and Technology* **46**: 5704–5712. https://doi.org/10.1021/es204247f.

Di Baldassarre G, Viglione A, Carr G, Kuil L, Salinas JL, Blöschl G. 2013. Socio-hydrology: Conceptualising human-flood interactions. *Hydrology and Earth System Sciences* **17**: 3295–3303. https://doi.org/10.5194/hess-17-3295-2013.

Dietze E, Hartmann K, Diekmann B, Ijmker J, Lehmkuhl F, Opitz S, Stauch G, Wunnemann B, Borchers A. 2012. An end-member algorithm for deciphering modern detrital processes from lake sediments of Lake Donggi Cona, NE Tibetan Plateau, China. *Sedimentary Geology* **243**: 169–180.

Dietze M, Dietze E. 2016. EMMAgeo: End-member modelling algorithm and supporting functions for grain-size analysis. In R package version 0.9.0.

Environment Agency. 2018. In *Estimating the economic costs of the 2015 to 2016 winter floods*, Agency E (ed), Vol. **50**. Environment Agency: Bristol.

Evin G, Wilhelm B, Jenny J-P. 2019. Flood hazard assessment of the Rhône River revisited with reconstructed discharges from lake sediments. *Global and Planetary Change* **172**: 114–123. https://doi.org/10.1016/j.gloplacha.2018.09.010.

Folk RL, Ward WC. 1957. Brazos River bar: a study in the significance of grain size parameters. *Journal of Sedimentary Research* **27**: 3–26.

Gray ST, Graumlich LJ, Betancourt JL, Pederson GT. 2004. A tree-ring based reconstruction of the Atlantic Multidecadal Oscillation since 1567 AD. *Geophysical Research Letters* **31**. https://doi.org/10.1029/2004gl019932.

Guha-Sapir D, Below R, Hoyois P. 2014. *EM-DAT: International disaster database*. Univ. Cathol. Louvain, Brussels: Belgium. www.em-dat.net. Accessed 20:

Håkanson L, Jansson M. 1983. *Principles of lake sedimentology*. Springer: Berlin.

Hall J, Arheimer B, Borga M, Brázdil R, Claps P, Kiss A, Kjeldsen TR, Kriauĉuniene J, Kundzewicz ZW, Lang M, Llasat MC, Macdonald N, McIntyre N, Mediero L, Merz B, Merz R, Molnar P, Montanari A, Neuhold C, Parajka J, Perdigão RAP, Plavcová L, Rogger M, Salinas JL, Sauquet E, Schär C, Szolgay J, Viglione A, Blöschl G. 2014. Understanding flood regime changes in Europe: A state-of-the-art assessment. *Hydrology and Earth System Sciences* **18**: 2735–2772. https://doi.org/10.5194/hess-18-2735-2014.

Hallegatte S, Green C, Nicholls RJ, Corfee-Morlot J. 2013. Future flood losses in major coastal cities. *Nature Climate Change* **3**: 802–806. https://doi.org/10.1038/nclimate1979.

Hannaford J, Marsh TJ. 2008. High-flow and flood trends in a network of undisturbed catchments in the UK. *International Journal of Climatology* **28**: 1325–1338.

Huntingford C, Marsh T, Scaife AA, Kendon EJ, Hannaford J, Kay AL, Lockwood M, Prudhomme C, Reynard NS, Parry S, Lowe JA, Screen JA, Ward HC, Roberts M, Stott PA, Bell VA, Bailey M, Jenkins A, Legg T, Otto FEL, Massey N, Schaller N, Slingo J, Allen MR. 2014. Potential influences on the United Kingdom's floods of winter 2013/14.

Nature Climate Change **4**: 769–777. https://doi.org/10.1038/nclimate2314.

Johnson R, Warburton J. 2006. Variability in sediment supply, transfer and deposition in an upland torrent system: Iron Crag, northern England. *Earth Surface Processes and Landforms* **31**: 844–861.

Kjeldsen TR, Jones DA. 2006. Prediction uncertainty in a median-based index flood method using L moments. *Water Resources Research* **42**. DOI: Artn W07414. https://doi.org/10.1029/2005wr004069.

Lavers DA, Allan RP, Wood EF, Villarini G, Brayshaw DJ, Wade AJ. 2011. Winter floods in Britain are connected to atmospheric rivers. *Geophysical Research Letters* **38**: n/a–n/a. https://doi.org/10.1029/2011gl049783.

Macdonald N, Kjeldsen TR, Prosdocimi I, Sangster H. 2014. Reassessing flood frequency for the Sussex Ouse, Lewes: the inclusion of historical flood information since AD1650. *Natural Hazards and Earth System Sciences* **14**: 2817–2828.

Macdonald N, Sangster H. 2017. High-magnitude flooding across Britain since AD 1750. *Hydrology and Earth System Sciences* **21**: 1631–1650. https://doi.org/10.5194/hessd-11-10157-2014.

Miller H, Croudace IW, Bull JM, Cotterill CJ, Dix JK, Taylor RN. 2014. A 500 year sediment lake record of anthropogenic and natural inputs to windermere (English Lake District) using double-spike lead isotopes, radiochronology, and sediment microanalysis. *Environmental Science and Technology* **48**: 7254–7263. https://doi.org/10.1021/es5008998.

Miller JD, Kjeldsen TR, Hannaford J, Morris DG. 2013. A hydrological assessment of the November 2009 floods in Cumbria, UK. *Hydrology Research* **44**: 180. https://doi.org/10.2166/nh.2012.076.

Mulder T, Alexander J. 2001. The physical character of subaqueous sedimentary density flows and their deposits. *Sedimentology* **48**: 269–299. https://doi.org/10.1046/j.1365-3091.2001.00360.x.

NERC. 1999. *Flood estimation handbook*. Institute of Hydrology: Wallingford.

NOAA. 2018. National Centers for Environmental Information, State of the Climate: Global Climate Report for Annual 2017.

Orr H, Davies G, Quinton J, Newson M. 2004. Bassenthwaite Lake Geomorphological Assessment Final Report. Unpublished report to the Environment Agency, June 2004.

Parry S, Barker L, Prosdocimi I, Lewis M, Hannaford J, Clemas S. 2016. Hydrological summary for the United Kingdom: December 2015.

Pennington W. 1981. Records of a lake's life in time: the sediments. *Hydrobiologia* **79**: 197–215. https://doi.org/10.1007/BF00006315.

Pennington W. 1991. Palaeolimnology in the English Lakes - some questions and answers over fifty years. *Hydrobiologia* **214**: 9–24. https://doi.org/10.1007/BF00050927.

R Core Team. 2017. *R: A language and environment for statistical computing*. R Foundation for Statistical Computing: Vienna Austria.

Robson A, Reed D. 1999. *Flood estimation handbook*. Institute of Hydrology: Wallingford.

Schillereff DN, Chiverrell RC, Boyle JF, Croudace IW. 2015. An intercomparison of μXRF scanning analytical methods. In *Developments in Palaeoenvironmental Research: Micro-XRF Studies of Sediment Cores*, Rothwell RG, Croudace IW (eds). Springer: Dordrecht; 110–120.

Schillereff DN, Chiverrell RC, Macdonald N, Hooke JM. 2014. Flood stratigraphies in lake sediments: A review. *Earth-Science Reviews* **135**: 17–37. https://doi.org/10.1016/j.earscirev.2014.03.011.

Schillereff DN, Chiverrell RC, Macdonald N, Hooke JM. 2016. Hydrological thresholds and basin control over paleoflood records in lakes. *Geology* **44**: 43–46. https://doi.org/10.1130/g37261.1.

Schulte L, Peña JC, Carvalho F, Schmidt T, Julià R, Llorca J, Veit H. 2015. A 2600-year history of floods in the Bernese Alps, Switzerland: Frequencies, mechanisms and climate forcing. *Hydrology and Earth System Sciences* **19**: 3047–3072. https://doi.org/10.5194/hess-19-3047-2015.

Shi F, Yang B, Mairesse A, von Gunten L, Li J, Bräuning A, Yang F, Xiao X. 2013. Northern Hemisphere temperature reconstruction during the last millennium using multiple annual proxies. *Climate Research* **56**: 231–244. https://doi.org/10.3354/cr01156.

Sjögren P, Edwards ME, Gielly L, Langdon CT, Croudace IW, Merkel MKF, Fonville T, Alsos IG. 2017. Lake sedimentary DNA accurately records 20th Century introductions of exotic conifers in Scotland. *New Phytologist* **213**: 929–941. https://doi.org/10.1111/nph.14199.

Stanley CJ, Vaughan DJ. 1982. Copper, lead, zinc and cobalt mineralization in the English Lake District: classification, conditions of formation and genesis. *Journal of the Geological Society* **139**: 569–579.

Stewart E, Morris D, Jones D, Gibson H. 2012. Frequency analysis of extreme rainfall in Cumbria, 16–20 November 2009. *Hydrology Research* **43**: 649–662.

Sutton RT, Dong B. 2012. Atlantic Ocean influence on a shift in European climate in the 1990s. *Nature Geoscience* **5**: 788–792. https://doi.org/10.1038/ngeo1595.

Thackeray S, Maberly S, Winfield I. 2010. The ecology of Bassenthwaite Lake (English Lake District)

Tyler I. 2003. *Carrock and the mines of Skiddaw and Blencathra*. Blue Rock Publications: Keswick.

Tyler I. 2005a. *Force Crag: the history of a Lakeland mine*. Blue Rock Publications: Keswick.

Tyler I. 2005b. *Goldscope and the mines of Derwent fells*. Blue Rock Publications: Keswick.

Warburton J. 2010. Sediment transfer in steep upland catchments (Northern England, UK): Landform and sediment source coupling. *Lecture Notes in Earth Sciences* **115**: 165–183. https://doi.org/10.1007/978-3-540-75761-0_11.

Wilby RL, Quinn NW. 2013. Reconstructing multi-decadal variations in fluvial flood risk using atmospheric circulation patterns. *Journal of Hydrology* **487**: 109–121.

Wilhelm B, Arnaud F, Sabatier P, Magand O, Chapron E, Courp T, Tachikawa K, Fanget B, Malet E, Pignol C, Bard E, Delannoy JJ. 2013. Palaeoflood activity and climate change over the last 1400 years recorded by lake sediments in the north-west European Alps. *Journal of Quaternary Science* **28**: 189–199. https://doi.org/10.1002/jqs.2609.

Wilhelm B, Ballesteros Canovas JA, Corella Aznar JP, Kämpf L, Swierczynski T, Stoffel M, Støren E, Toonen W. 2018a. Recent advances in paleoflood hydrology: From new archives to data compilation and analysis. *Water Security* **3**: 1–8. https://doi.org/10.1016/j.wasec.2018.07.001.

Wilhelm B, Ballesteros Cánovas JA, Macdonald N, Toonen WHJ, Baker V, Barriendos M, Benito G, Brauer A, Corella JP, Denniston R, Glaser R, Ionita M, Kahle M, Liu T, Luetscher M, Macklin M, Mudelsee M, Munoz S, Schulte L, St. George S, Stoffel M, Wetter O. 2018b. Interpreting historical, botanical, and geological evidence to aid preparations for future floods. *Wiley Interdisciplinary Reviews Water* **6**. https://doi.org/10.1002/wat2.1318.

Wong JS, Freer JE, Bates PD, Sear DA, Stephens EM. 2015. Sensitivity of a hydraulic model to channel erosion uncertainty during extreme flooding. *Hydrological Processes* **29**: 261–279.